ChemComm

www.rsc.org/chemcomm

COMMUNICATION

Hanging Pt hollow nanocrystal assemblies on graphene resulting in an enhanced electrocatalyst†

Yu-Ping Xiao,[ab] Shuo Wan,[c] Xing Zhang,[a] Jin-Song Hu,*[a] Zi-Dong Wei*[b] and Li-Jun Wan*[a]

Pt hollow nanostructures assembled by nanocrystals were *in situ* grown and hung onto graphene layers to combine the merits from favorable catalyst morphology control and synergetic improvement effect of the graphene support, resulting in a composite with enhanced electrocatalytic performance.

The rapidly increasing energy demand for human activities necessitates continuous research interests to develop renewable energy alternatives worldwide. Proton exchange membrane fuel cells (PEMFCs) and direct methanol fuel cells (DMFCs) are two options for clean energy to catalytically transform chemical energy directly into electricity instead of burning natural resources at the cost of the environment. The big challenge for the practical application of these two techniques is to minimize the use and maximize the catalytic activity of scarce, expensive catalysts such as platinum, still the best electrocatalyst to date.[1,2] Several strategies have been explored to achieve this goal, including optimizing the size and shape of Pt nanoparticles;[3–5] developing Pt nanoparticles with high energy facets;[6–8] alloying it with other transition metals such as Au, Ni, Co and Pd *etc.*;[9–13] as well as supporting Pt nanoparticles onto catalyst supports such as carbon or carbon nanotubes *etc.*

Graphene, as a two-dimensional (2D) sheet with fully delocalized π-electrons, has been successfully used as a new 2D support in catalytic applications although undoped graphene itself does not show catalytic activity. The close contact of graphene with catalysts is believed to play an important role in the enhancement of catalytic performance of catalysts, as demonstrated in Pt- or Pd-based graphene materials, for Co_3O_4 nanoparticles grown on graphene, as well as FePt nanoparticle-assembled graphene.[14–16] There are usually two routes to load catalysts on graphene supports: direct growth and assembly of as-synthesized catalyst. The direct growth of nanoparticles on the graphene surface can maximize the graphene–nanoparticle contact to achieve the performance enhancement but often leads to poor control of the desired size and morphology of catalyst particles. Oppositely, the assembly of synthesized nanoparticles on graphene results in superior size and shape controllability of catalysts but usually requires surfactant, which could block the active catalytic sites of catalysts and their effective contact with graphene, and thus may require post-thermal treatment with a risk of catalyst agglomeration. Therefore, developing surfactant-free strategies to *in situ* assemble platinum nanoparticles with desired size, morphology and structure control on graphene would be the ideal way to effectively utilize graphene as a 2D catalyst mat with the potential to harness the unique properties of graphene for designing next-generation catalysts.

The idea here is to use sacrificeable metal nanoparticles grown on graphene to *in situ* achieve Pt nanocrystal assemblies with hollow interiors hung on graphene (designated as Pt–H–G), which displays the controllability of favorable catalyst morphology and structure as well as close contact between catalyst nanoparticles and graphene for effectively accomplishing the synergetic effect of graphene as catalyst support. As demonstrated below by the enhanced electrocatalytic activities for methanol oxidation reaction (MOR), the reported Pt–H–G catalyst shows the following advantages: (1) efficient catalyst utilization, reduction of cost, low density, and effective mass transfer from the hollow structures; (2) synergetic improvement effect from graphene; (3) desirable size of nanocrystals with an average diameter of 3.5 nm for maximal catalytic performance;[3] (4) appropriate size of hollow assemblies of around 20 nm to effectively prevent nanocrystal aggregation and active surface loss due to graphene wrapping, yet retention of close contact between catalyst nanocrystals and graphene.

Pt–H–G was synthesized by *in situ* galvanic replacement of Co nanoparticles grown onto graphene sheets at room temperature. The formation process of Pt–H–G is illustrated in Fig. 1. In brief, graphene oxide (GO) was synthesized by the modified Hummers method, and then treated in H_2/Ar gas at 800 °C, followed by functionalization in nitric acid (see ESI†). When $CoCl_2$ solution was added into functionalized graphene aqueous suspension, cobalt ions were absorbed on the negatively charged graphene sheets. After the addition of $NaBH_4$, cobalt ions were reduced to form Co nanoparticles on the graphene layers. When H_2PtCl_6 was added, the galvanic replacement reaction instantly occurred between $PtCl_6^{2-}$ and Co^{2+} due to the much higher standard reduction potential of the $PtCl_6^{2-}$/Pt redox pair (0.735 V *vs.* SHE) than that of the Co^{2+}/Co redox pair (0.277 V *vs.* SHE). The reaction led to the nucleation and growth of Pt nanocrystals around Co nanoparticles. As the

[a] *Key Laboratory of Molecular Nanostructure and Nanotechnology, Institute of Chemistry, Chinese Academy of Sciences, Beijing 100190, China. E-mail: hujs@iccas.ac.cn, wanlijun@iccas.ac.cn*
[b] *Department of Chemistry and Chemical Engineering, Chongqing University, Chongqing, 400044, China. E-mail: zdwei@cqu.edu.cn*
[c] *College of Chemistry and Chemical Engineering, Xiamen University, Xiamen 361005, China*
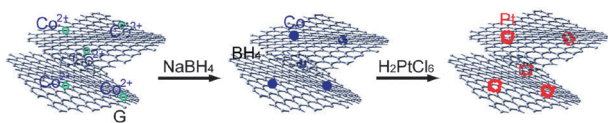† Electronic supplementary information (ESI) available. See DOI: 10.1039/c2cc35562k

Fig. 1 Schematic illustration for the formation of Pt nanoparticle assemblies with hollow interiors on graphene sheets.

reaction proceeded, Co was continuously consumed to eventually form a hollow interior, accompanied by the formation of Pt hollow nanostructures assembled by Pt nanocrystals. Because Co nanoparticles were grown in graphene layers, the resultant Pt nanocrystal assemblies with hollow interiors replaced them and were hung on the graphene sheets.

The morphologies and structure of the synthesized Pt–H–G were first investigated *via* scanning electron microscopy (SEM) and transmission electron microscopy (TEM). Fig. 2a shows a typical SEM image of Pt–H–G. It is clearly seen that many spherical particles with higher contrast and diameter of around 20 nm are decorated on the layered materials. As confirmed by the energy dispersed spectrum (EDS) shown in Fig. S1†), these nanospheres are made of Pt. The inset in Fig. 2a presents a high magnification SEM image of a single Pt nanosphere, demonstrating the nanosphere indeed consists of many smaller nanoparticles of diameter *ca.* 3–4 nm. Moreover, it is also shown in SEM images (Fig. 2a and S2†) that the Pt nanospheres are well distributed on graphene with some above the graphene sheets and some intercalated in layers, as implied by the contrast difference. TEM images shown in Fig. 2b and c reveal that all these nanoparticles have hollow interiors as manifested by the obvious contrast difference in terms of darker edges and lighter centers. The high magnification TEM image (Fig. 2c) also shows the shells of these Pt nanoparticles are assembled by smaller nanocrystals, consistent with the result from SEM images. Fig. 2d presents a typical high-resolution TEM image of a part of nanosphere, clearly showing the lattice fringes with a *d* spacing of 0.23 nm corresponding to the (111) plane distance of face-centered cubic (fcc) crystalline Pt. The selected-area electron diffraction (SAED) pattern (Fig. S3†) gives diffraction rings also agreeing with fcc Pt crystals. To further identify the crystal structure and evaluate the average size of nanocrystals, the powder X-ray diffraction (XRD) pattern of Pt–H–G was recorded as shown in Fig. 3a. Four major peaks can be indexed well to (111), (200), (220) and (311) planes of cubic structure
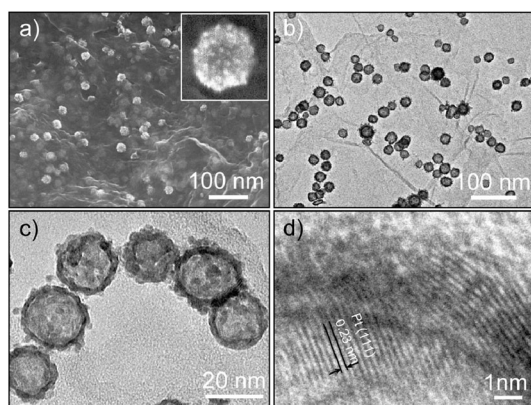
Pt (JCPDS 04-0802). The average size of Pt nanocrystals was calculated to be 3.46 nm, according to the Scherrer formula from the half-peak width for Pt(220), in good agreement with SEM and TEM results. The wide XRD peak at around 25° could be ascribed to the graphene (002) plane. The graphene features can be also seen in SEM and TEM images. The wrinkled folds shown in Fig. 2a and dark lines in Fig. 2b are typical features of graphene layers. In order to further investigate the nature of graphene in Pt–H–G, the Raman spectrum was measured on Pt–H–G at room temperature with 633 nm excitation. As shown in Fig. 3b, the typical Raman spectrum of Pt–H–G shows three most intense features at 1347, 1578 and 2684 cm^{-1}, which can be attributed to the D, G and 2D bands of graphene, respectively.[17] The D band at 1347 cm^{-1} probably originates from symmetry-breaking at the graphene edges or possible defects on graphene due to functionalization treatment.[17] It is known that the G and 2D bands in Raman spectra can be used to evaluate the number of graphene layers. By comparing the position, shape and intensity ratio of the obtained G and 2D peaks with literature values, it can be concluded that graphene sheets in Pt–H–G reported here are mostly composed of 5–10 layers.[17]

In order to evaluate the electrocatalytic activity of Pt–H–G and the improvement effect of graphene in catalyst performance, unsupported Pt hollow nanospheres (Pt–H) were also prepared under the same condition as that for Pt–H–G but without the addition of graphene. TEM image and the SAED pattern shown in Fig. S4† confirm that Pt–H has a similar morphology and structure to the Pt hollow nanocrystal assemblies in Pt–H–G. The electrocatalytic performance of Pt–H–G (44% Pt based on TGA, Fig. S5†) was first evaluated by measuring its electrocatalytic activity for methanol oxidation reaction in 0.5 M H$_2$SO$_4$–0.5 M methanol, and comparing with that of Pt–H, commercial Pt/C catalyst (40% Pt), and Pt black. Before the measurement, the electrochemically active surface areas (ECSA) of all catalysts were measured. It was found that ECSA of Pt–H–G (13.0 m^2 g^{-1}) was ~1.3 times that of Pt–H (10.6 m^2 g^{-1}) probably due to the good dispersion of Pt–H on graphene. Fig. 4a presents the ECSA specific electrocatalytic activity of the four tested catalysts for MOR. It is clearly seen that Pt–H–G shows the highest methanol oxidation current with a peak current of 1.68 mA cm^{-2}, which is ~4 times that of commercial Pt/C (0.41 mA cm^{-2}), ~12 times that of commercial Pt black (0.14 mA cm^{-2}), and ~1.6 times that of Pt nanoparticles/graphene catalysts with the same Pt loading and similar Pt size (measured in 2 M methanol).[18] Interestingly, it should be noted that the specific MOR electrocatalytic activity of Pt–H–G was much improved by ~2.75 times as compared to Pt–H catalysts with no graphene as catalyst support, indicating a significant
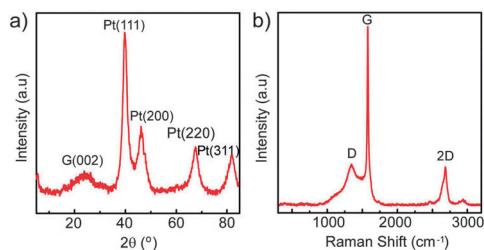

Fig. 2 Low- (a) and high-magnification (inset in a) SEM images of Pt–H–G. Low- (b), high-magnification (c), and high resolution (d) TEM images of Pt–H–G.

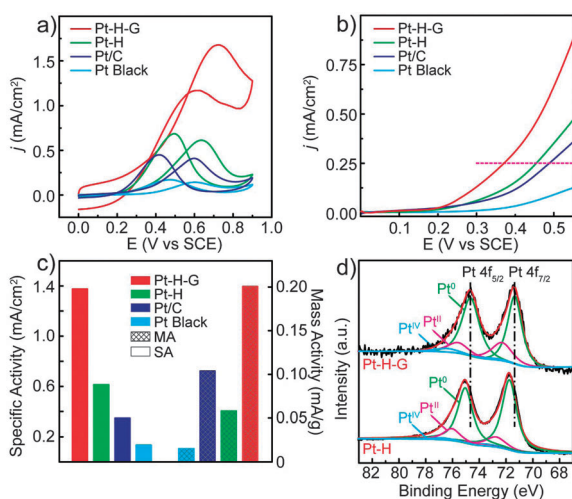**Fig. 3** XRD pattern (a) and Raman spectrum (b) of Pt–H–G.

Fig. 4 (a) Cyclic voltammograms and (b) linear-sweep voltammograms curves for MOR catalysed by Pt–H–G (red), Pt–H (green), commercial Pt/C (blue) and Pt black (cyan) in aqueous solution containing 0.5 M H_2SO_4 and 0.5 M methanol. The effect of the double-layer in Pt–H–G was corrected for. (c) Comparison of MOR area specific activity (left) and mass activity (right) of the four catalysts, calculated from MOR current in CV curves obtained at 0.65 V (vs. SCE) and ECSA and mass of the used catalysts, respectively. (d) XPS spectra of Pt–H–G and Pt–H in the Pt 4f region.

synergetic effect of graphene for MOR. Moreover, as indicated by the dashed line in Fig. 4b, the oxidation potentials on Pt–H–G are obviously lower than those on Pt–H, Pt/C and Pt black at applicable oxidation current density. For example, the oxidation potential on Pt–H–G was negatively shifted by 117 mV relative to that on Pt/C, and by 83 mV relative to Pt–H at a current density of 0.25 mA cm^{-2}, further indicating that the methanol oxidation reaction was easier on Pt–H–G catalyst, and that graphene promoted the reaction. In order to directly compare the electrocatalytic activities of all evaluated catalysts for MOR, both specific activity and mass activity for electro-oxidation of methanol were calculated through dividing the oxidation current at 0.65 V (vs. SCE) by the ECSA and mass of four catalysts, respectively (Fig. 4c). It is shown that Pt–H–G delivered ~2.3 times larger area specific activity and ~3.5 times larger mass activity at the given potential compared with Pt–H. The former could be mainly attributed to the synergetic improvement for MOR from graphene while the latter could be ascribed to the synergetic effect of graphene as well as better dispersion of catalyst nanoparticles in Pt–H–G, which will result in larger ECSA at the same catalyst loading. To further elucidate the synergetic improvement from graphene for MOR, X-ray photoelectron spectra (XPS) were measured on Pt–H–G and Pt–H. Fig. 4d shows the Pt 4f signals were deconvoluted into three components as usual. By comparing the two spectra, it can be seen that the binding energies for both Pt 4f$_{5/2}$ and 4f$_{7/2}$ peaks in Pt–H–G both negatively shifted by ~0.40 eV relative to Pt–H, indicating the electronic structure of Pt atoms were affected to some extent by graphene and implying the electron transfer from graphene to Pt.[19,20] According to literature and d-band center theory, the change in the binding energy of the metal core level reflects the shift of its d-band center relative

Fermi level, which will affect the adsorption energy of adsorbates on the metal surface.[19–21] The change in charge state of the Pt core and in adsorption energy of adsorbates on its surface are believed to contribute to the enhancement of MOR activity, although further experiments and analysis are needed to clarify the results.

In summary, a facile method has been developed to synthesize and in situ hang Pt hollow nanostructures on graphene, whose shells were assembled by small nanoparticles set to a suitable size for electrocatalytic applications. As a result of controlling the favorable catalyst morphology and simultaneously retaining close contact between catalyst and graphene, the synthesized Pt-graphene hybrid catalysts combined the merits from nanocrystal assembled hollow structures and the synergetic improvement effect of the graphene support, and thus exhibited enhanced electrocatalytic activities for MOR. It is believed that further optimization for the size and the content of Pt nanostructures on graphene could further improve the electrocatalytic activity of Pt–H–G.

References

1 M. K. Debe, Nature, 2012, **486**, 43.
2 A. Rabis, P. Rodriguez and T. J. Schmidt, ACS Catal., 2012, **2**, 864.
3 F. J. Perez-Alonso, D. N. McCarthy, A. Nierhoff, P. Hernandez-Fernandez, C. Strebel, I. E. L. Stephens, J. H. Nielsen and I. Chorkendorff, Angew. Chem., Int. Ed., 2012, **51**, 4641.
4 S. H. Sun, G. X. Zhang, D. S. Geng, Y. G. Chen, R. Y. Li, M. Cai and X. L. Sun, Angew. Chem., Int. Ed., 2011, **50**, 422.
5 B. Y. Xia, W. T. Ng, H. B. Wu, X. Wang and X. W. Lou, Angew. Chem., Int. Ed., 2012, **51**, 7213.
6 N. Tian, Z. Y. Zhou, S. G. Sun, Y. Ding and Z. L. Wang, Science, 2007, **316**, 732.
7 A. X. Yin, X. Q. Min, Y. W. Zhang and C. H. Yan, J. Am. Chem. Soc., 2011, **133**, 3816.
8 T. Yu, D. Y. Kim, H. Zhang and Y. N. Xia, Angew. Chem., Int. Ed., 2011, **50**, 2773.
9 B. Lim, M. J. Jiang, P. H. C. Camargo, E. C. Cho, J. Tao, X. M. Lu, Y. M. Zhu and Y. N. Xia, Science, 2009, **324**, 1302.
10 J. Zhang, K. Sasaki, E. Sutter and R. R. Adzic, Science, 2007, **315**, 220.
11 J. B. Wu, J. L. Zhang, Z. M. Peng, S. C. Yang, F. T. Wagner and H. Yang, J. Am. Chem. Soc., 2010, **132**, 4984.
12 V. R. Stamenkovic, B. Fowler, B. S. Mun, G. F. Wang, P. N. Ross, C. A. Lucas and N. M. Markovic, Science, 2007, **315**, 493.
13 J. Zhang, H. Z. Yang, J. Y. Fang and S. Z. Zou, Nano Lett., 2010, **10**, 638.
14 Y. Y. Liang, Y. G. Li, H. L. Wang, J. G. Zhou, J. Wang, T. Regier and H. J. Dai, Nat. Mater., 2011, **10**, 780.
15 S. J. Guo, S. J. Dong and E. K. Wang, ACS Nano, 2010, **4**, 547.
16 S. J. Guo and S. H. Sun, J. Am. Chem. Soc., 2012, **134**, 2492.
17 A. C. Ferrari, J. C. Meyer, V. Scardaci, C. Casiraghi, M. Lazzeri, F. Mauri, S. Piscanec, D. Jiang, K. S. Novoselov, S. Roth and A. K. Geim, Phys. Rev. Lett., 2006, **97**, 187401.
18 J. D. Qiu, G. C. Wang, R.-P. Liang, X. H. Xia and H. W. Yu, J. Phys. Chem. C, 2011, **115**, 15639.
19 H. Tsunoyama, N. Ichikuni, H. Sakurai and T. Tsukuda, J. Am. Chem. Soc., 2009, **131**, 7086.
20 J. Greeley, J. K. Nørskov and M. Mavrikakis, Annu. Rev. Phys. Chem., 2002, **53**, 319.
21 M. Wakisaka, S. Mitsui, Y. Hirose, K. Kawashima, H. Uchida and M. Watanabe, J. Phys. Chem. B, 2006, **110**, 23489.